JOURNAL OF QUATERNARY SCIENCE (2020) **35**(4) 582–593 ISSN 0267-8179. DOI: 10.1002/jqs.3201

JQS Journal of Quaternary Science QRA Quaternary Research Association

A 180 ka record of environmental change at Erdut (Croatia): a new chronology for the loess–palaeosol sequence and its implications for environmental interpretation

KAJA FENN,[1]* JULIE A. DURCAN,[1] DAVID S. G. THOMAS[1] and ADRIANO BANAK[2]
[1]Oxford University Centre for the Environment, UK
[2]Croatian Geological Survey, Department of Geology, Croatia

Received 2 May 2019; Revised 27 March 2020; Accepted 28 March 2020

ABSTRACT: While there are numerous thick loess–palaeosol sequences preserved across the Carpathian Basin, well dated sites that provide terrestrial palaeoenvironmental records extending beyond last glacial–interglacial cycle are scarce. Robust chronologies are essential for correlations of loess with other long-term Quaternary records and to further understanding of the palaeoenvironment and climate of this important region beyond the last 125 ka. Here a new geochronology based on 13 post-infrared infrared stimulated luminescence ages focused on the lower part of the loess–palaeosol sequence at Erdut is presented. The results show that the lower part of the Erdut profile spans the penultimate glacial cycle (MIS 7 to MIS 5). The considerable sediments overlaying the investigated part of the profile suggest that this section spans two glacial cycles, rather than the previously suggested one. The most likely source of the discrepancy is the use of uncorrected infrared stimulated luminescence signal, which can cause age underestimation if not accounted for. This study demonstrates the need to revisit sites such as Erdut, re-date them using updated measurement protocols, and update existing palaeoenvironmental interpretations. © 2020 The Authors. *Journal of Quaternary Science* Published by John Wiley & Sons Ltd

KEYWORDS: luminescence dating; MARs; MIS 6; pIRIR; Quaternary.

Introduction

Loess–palaeosol sequences are important terrestrial archives often preserving near-continuous and high-resolution sedimentary records. They often span multiple glacial–interglacial cycles and offer long-term Quaternary records in regions where other long-term archives are frequently absent. Therefore they provide a unique insight into the Earth's past and an opportunity to compare and correlate terrestrial signals with ice- and marine- core records (Kukla, 1977; Antoine *et al.*, 2009; Stevens *et al.*, 2018).

Central European loess deposits, especially along the Danube River, are particularly thick, with a number of sites extending beyond the last glacial–interglacial cycle, including in Bulgaria (Jordanova *et al.*, 2008), Croatia (Galović *et al.*, 2009; Wacha and Frechen, 2011), Hungary (Thiel *et al.*, 2014; Újvári *et al.*, 2014), Romania (Balescu *et al.*, 2010; Vasiliniuc *et al.*, 2012), and Serbia (Schmidt *et al.*, 2010; Murray *et al.*, 2014). Consequently, in terms of capacity to generate long palaeoclimate and palaeoenvironment signals in central and southeastern Europe, loess archives are only matched by a very limited number of lacustrine records, e.g. Lake Ohrid, Macedonia (Lacey *et al.*, 2016), Tenaghi Philippon, Greece (Tzedakis *et al.*, 2006), or Lake Ioannina, Greece (Roucoux *et al.*, 2011).

Despite their potential as palaeoarchives, loess–palaeosol sequences often suffer from a lack of robust, high-resolution, absolute chronologies. Traditionally, researchers have relied on broad stratigraphy, e.g. position and number of palaeosols (Marković *et al.*, 2015), geomagnetic polarity reversal tie points (Marković *et al.*, 2011; Sümegi *et al.*, 2018), and sedimentological correlations with distant ice cores (An, 2000; Rousseau *et al.*, 2002; Antoine *et al.*, 2009). However, these methods assume continuous deposition and the absence of erosion, which has since been shown to be erroneous (Stevens *et al.*, 2006, 2018). In addition, stratigraphic correlation has proven more complicated than originally thought, for example, single soils corresponding to multiple soils at other sites (Marković *et al.*, 2008), and has led to ambiguous links (*cf* Thiel *et al.*, 2014). A reliable and independent chronology is therefore accepted as a critical underpinning of studies covering the last glacial–interglacial period, and by extension wherever possible the same requirement should be applied to studies extending beyond 125 ka.

In theory, infrared stimulated luminescence (IRSL) dating of feldspar provides the potential to date 300–500-ka-old material (Thomsen *et al.*, 2011), because of feldspars' higher saturation limit. They therefore provide the opportunity to construct chronologies for loess profiles extending beyond the last interglacial period (e.g. Novothny *et al.*, 2002; Schmidt *et al.*, 2010; Wacha and Frechen, 2011). However, some feldspar signals are athermally unstable, a phenomenon termed 'anomalous fading' (Wintle, 1973). This process causes feldspars to 'leak' signal and results in age underestimation if not corrected for. Although corrections for the signal loss are possible (Lamothe and Auclair, 1999; Huntley and Lamothe, 2001), they can be problematic and are mainly applicable to younger samples. In 2008, Thomsen *et al.* published a post-infrared infrared (pIRIR) measurement protocol for potassium feldspar signals, which allows a more stable signal to be accessed. Subsequently, a number of studies across the region have tested the pIRIR protocol and when compared with independent age controls such as tephra (Thiel *et al.*, 2011b), radiocarbon ages within the last 50 ka (Thiel *et al.*, 2011a; Újvári *et al.*, 2014), or semi-independent

*Correspondence: K. Fenn, as above.
E-mail: kaja.fenn@ouce.ox.ac.uk

quartz optically stimulated luminescence (OSL) ages (Buylaert *et al.*, 2011; Schatz *et al.*, 2012), they showed the ability to accurately date loess sites extending beyond 70 ka.

Here a new pIRIR luminescence geochronology based on 13 ages for the loess–palaeosols section at Erdut, Croatia, is presented. A nearby section was investigated by Galović *et al.* (2009), but their study relied on only five luminescence ages, calculated using an additive-dose IRSL protocol. This protocol can result in large age uncertainties (Novothny *et al.*, 2010; Wacha *et al.*, 2011), and in their study, Galović *et al.* (2009) did not investigate or correct their IRSL signals for fading, generating the potential for age underestimation.

Geological setting and site description

Loess deposits in eastern Croatia are primarily found along the Danube River valley where a number of thick sequences have been reported (Wacha and Frechen, 2011; Banak *et al.*, 2012; Wacha *et al.*, 2013). Erdut (45°30′49.78″N, 19°4′39.072″E, 97 m a.s.l.) is located on the western bank of the Danube (Fig. 1), 150 m from an abandoned channel and 1.2 km from the modern river. Loess–palaeosol sequences at the site are associated with a very small (~30 km^2) plateau-like feature, which follows the bend of the Danube River. The feature is heavily incised by gullies on the northern side, while on the southern side, exposures are not as extensive or thick. The loess outcrops on the southern side are situated on a gentle slope towards the river, with individual unit thickness decreasing in the same direction.

Investigated outcrop comprises three palaeosol and three loess units, one of which is punctuated by a laminated sediment (Table 1 and Fig. 2). The top four units (Unit I – modern soil, Unit II, Unit III and Unit IV) were not sampled in this study. Unit V comprises a pale brown soil (10YR 6/3) with small, granular peds and numerous small shells. Unit VI, a thick loess layer, has a high concentration of well-preserved gastropods, 1 mm – 2 cm in size, especially in its upper 2.5 m (Fig. 3B). The sediment is pale yellow (2.5Y 7/3), though it gradually becomes yellowish brown (2.5YR 6/4) within the first metre. The field assessment suggests that the unit coarsens downwards from silt to sandy silt. The laminated sediment, Unit VII, comprises three sub-layers: horizontal lamination (30 cm), cross lamination (10 cm) and horizontal lamination (80 cm) again. In both cases, horizontal laminations comprise sheets a few millimetres thick of alternating silt and very fine sand (Fig. 3A). The cross laminations are also a few millimetres in thickness.

The final light yellowish brown loess (2.5Y 6/4) layer (Unit VIII) is mottled throughout and full of calcified root holes. The section culminates in a light reddish brown to lightly yellowish brown clayish palaeosol (10YR 6/4 to 2.5YR 6/3). The unit grades over 1 m from loess to a full soil. The total thickness of this unit could not be established as the profile could not be excavated fully.

Sampling, preparation and equipment

Due to access restrictions, only the lower parts of the Erdut profiles were accessible. Thirteen samples for grain size analysis (Supplementary Fig. S1) and age determination were collected (Fig. 2) using light-tight plastic cylinders. All samples for luminescence dating were handled under subdued orange-light conditions at the Oxford Luminescence Dating Laboratory, University of Oxford. The light-exposed sediment from both ends of the cylinder was removed and retained for dose rate and particle size analysis. Prior to sieving, all samples were pre-treated with 32% HCl to remove carbonates, and 30% H_2O_2 to remove organic matter. Samples were sieved to retain fine sand (63–90 μm), and density separated using sodium polytungstate to obtain potassium feldspar ($\rho < 2.58$ g cm^{-3}). Small (2 mm) coarse-grained aliquots were made by mounting a monolayer of sediment on the disc using silicone oil. All measurements were carried out using a Risø TL/OSL luminescence reader with a calibrated $^{90}Sr/^{90}Y$ beta source, and a bialkali photomultiplier tube. Potassium feldspar grains were stimulated with infrared-emitting diodes emitting at 870 nm, and signals were detected in the blue–violet region of the electromagnetic spectrum through a combination of Schott BG39/Corning 7-59 filters.

Thomsen *et al.* (2008) and Buylaert *et al.* (2012) have shown that the pIRIR signal measured at an elevated temperature is more stable over Quaternary timescales, and typically fades substantially less than the IR signal. Therefore, a pIRIR single aliquot regenerative dose (SAR) protocol was used for all measurements and D_e determination (Supplementary Table S1). After a 250 °C preheat, IR_{50} and $pIRIR_{elev}$ signals were measured for 200 s, followed by the measurement of a test

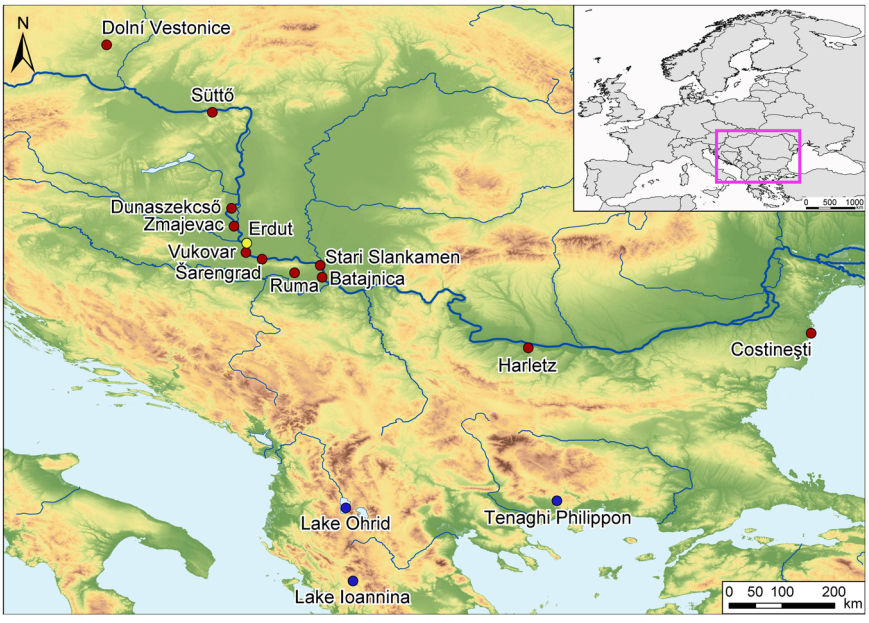

Figure 1. Map of the study region, study site (Erdut) and other sites discussed in the text. Yellow denotes Erdut, red other loess profiles, and blue lake sites (DEM Source: ©JAXA). [Color figure can be viewed at wileyonlinelibrary.com]

Table 1. The field description of the sedimentary units of all profiles at Erdut.

Unit	Section and depth (m)	L-P stratigraphy	Field description
I	**Erdut 4:** -	S0	*Modern Soil* Only observed at a distance. Therefore, unsure of the exact depth, colour, or
II	**Erdut 4:** -	L1LL1	*Loess* sedimentary structures in these units.
III	**Erdut 4:** -	L1SS1	*Palaeosol*
IV	**Erdut 4:** -	L1LL2	*Loess*
	Erdut 3: -		
V	**Erdut 4:** 3.3-4	S1	*Palaeosol:* At both profiles (Erdut 3 and 4) unit's structure is made of small granular peds (Fig. 3C). Palaeosol is pale brown (10YR 6/3), clayey and compacted. Small (<1 cm) unidentified gastropod shells (Fig. 3C) abundant throughout, while small insect burrows become abundant from 3.7 m. Both boundaries are irregular but quite sharp.
	Erdut 3: 3.2-4		At Erdut 4 the unit is slightly thinner (70 cm). Top and bottom boundaries are sharp and irregular.
VI	**Erdut 4:** 4-9.2	L2	*Loess:* At Erdut 3 the loess is pale yellow (2.5Y 7/3) dry and silty. The sediment is very compacted and cemented in the top 10 cm. Sediment shifts to light yellowish brown (2.5YR 6/4) at ~5.7 m.
	Erdut 3: 4-6.5		An assemblage of large gastropods (2–3 cm; Fig. 3B) is observed between 4 and 5 m. While a second assemblage of much smaller gastropod shells (max 1 cm) is noted between 5.6 and 6.1 m.
	Erdut 2: -		At Erdut 4 the same colour changes from pale yellow (2.5Y 7/3) to light yellowish brown (2.5YR 6/4) are observed. As with Erdut 3, gastropod assemblages of varying sizes (mm to 2 cm) are abundant between 5.7 and 6.4 m. Additionally, between 7.5 and 8.2 m small (1 cm) to large (>30 cm) carbonate concretions are observed.
	Erdut 1: -		While visible at Erdut 1 and 2 these units have only been observed at a distance. Therefore thickness and sedimentological description is unavailable.
VII	**Erdut 2**: 2.4-4	N/A	*Sandy and laminated complex:* At Erdut 1 a 50 cm unit of horizontally laminated silt and very fine sand with sharp top and bottom boundary is observed. The unit's thickness is not uniform laterally and shifts to 70 cm away from the river.
			At Erdut 2 Unit VII is 1.6 m thick and comprises four subunits: sandy layer (VIIa), horizontal laminations (VIIb), cross laminations (VIIc), and horizontal laminations (VIId).
			2.4–2.8 m. VIIa subunit is 40 cm thick of very fine, light olive brown (2.5Y 5/4).
	Erdut 1: 3.1-3.8		2.8–3.1 m. VIIb preserves 30 cm thick horizontal laminations of silt and very fine sand – mm in size and pale yellow (2.5Y 7/4) in colour. Sharp boundary with subunit above and below.
			3.1–3.2 m. VIIc comprise cross-laminated silt and very fine sand (10 cm). Sharp boundary with subunit above and below.
			3.2–4 m. VIId subunit contains 80 cm thick horizontally laminated silt and very fine sand, pale yellow (2.5Y 7/4). At ~3.7 m multiple large (20–30 cm) multiple calcrete precipitations are seen. Sharp boundary with loess below.
VIII	**Erdut 2:** 4-6.6	L2	*Loess:* At Erdut 1 profile unit comprises predominantly lightly yellowish brown (2.5Y 6/4) silt though very fine sand is also present especially within the first 10 cm from the boundary. Dark Fe/Mn and lighter $CaCo_3$ mottles present throughout the unit though they increase gradually down section.
	Erdut 1: 3.8-7.1		At Erdut 2 Unit VIII is also predominantly silty with no obvious structures. Below 5 m insect burrows become very abundant.
IX	**Erdut 1:** 7.1-8.7	S2	*Palaeosol:* Gradual transition into palaeosol (7.1–7.6 m). Fairly clayey, lightly reddish brown (2.5YR 6/4) silt with dark Fe/Mn and lighter $CaCo_3$ mottles.
			Main palaeosol noted from 7.6 m based on the gradually increasing clay content to silty clay and shift in colour to lightly yellowish brown (10YR 6/4). The boundary between the two parts is defused but straight.

dose to monitor sensitivity change. A 290 °C 'hot bleach' was performed at the end of each SAR cycle for 200 s. The signal was integrated from the first 2 s of the stimulation time subtracting the last 100 s of the background. The dose–response curves were fitted with an exponential function.

Dose rate determination

Environmental dose rates were calculated from radionuclide concentrations (U, Th, K and Rb) measured using inductively coupled plasma mass spectrometry at the British Geological Survey, Keyworth. Secondary standards were periodically measured to monitor analytical precision and accuracy. Radionuclide concentrations for each sample were converted to infinite-matrix dose rates using the Guérin *et al.* (2011) conversion factors. The infinite-matrix dose rates were adjusted for alpha efficiency using an a-value of 0.15 ± 0.05 (Balescu and Lamothe, 1994), grain size attenuation using the data set of Brennan *et al.* (1991) for alpha dose rates and Mejdahl (1979) for beta dose rates, and a commonly used loess moisture content of $15 \pm 5\%$ (Novothny *et al.*, 2009; Stevens *et al.*, 2011; Schatz *et al.*, 2012; Újvári *et al.*, 2014). Cosmogenic radiation contributions were corrected for sediment thickness and altitude (Prescott and Hutton, 1994). The internal dose rate was calculated in addition to the external dose rate using an internal potassium concentration of $12.5 \pm 0.5\%$ (Huntley and Baril, 1997). Dose rate calculation was carried out using DRAC (v1.2) software (Durcan *et al.*, 2015).

Equivalent dose determination

Preheat test/temperature selection

It has been suggested that the first IRSL stimulation temperature may impact pIRIR signal stability (Jain and Ankjærgaard, 2011). To test this, a prior-IR stimulation plateau test was conducted (Buylaert *et al.*, 2012), to ascertain the dependence of pIRIR D_e on the first IRSL measurement. Five temperatures (50–170 °C) were tested for the first IRSL stimulation while the pIRIR

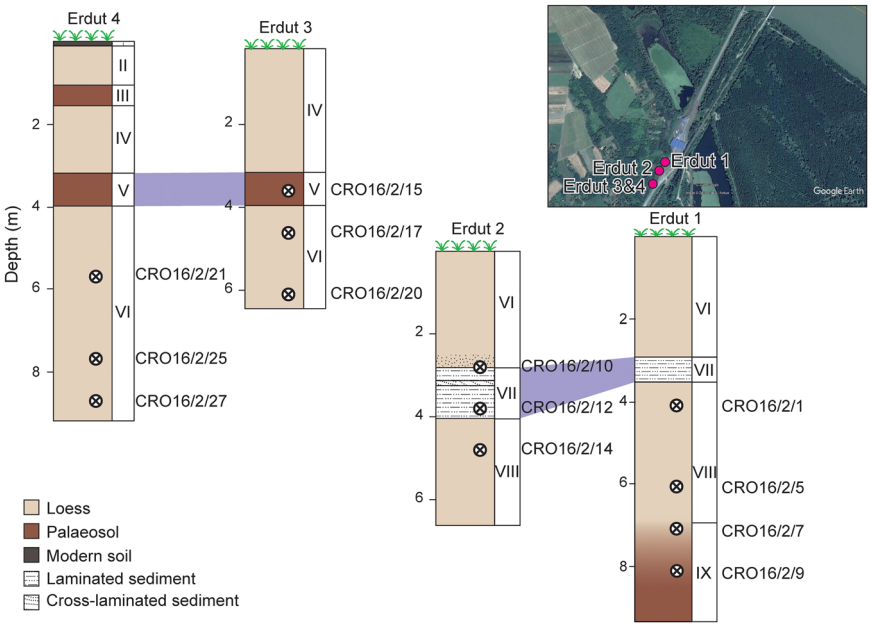

Figure 2. Stratigraphic logs of four profiles along a 100 m stretch of the exposure at Erdut. Sequences are 6, 60 and 20 m apart. Correlations between sections are based on the field observations and luminescence ages. Circles mark the position of the luminescence samples, and the field description of Units I–IX are given in Table 1. Insert shows the location of all four profiles in relation to each other (Source: ©GoogleEarth). [Color figure can be viewed at wileyonlinelibrary.com]

stimulation temperature was kept at 225 °C. Fig. 4 demonstrates that D_e is insensitive to the prior-IR stimulation temperature. However, because signal intensity diminishes with an increased IRSL temperature (Fig. 4, inset), 50 °C was selected for the IRSL stimulation in this study.

Roberts (2012) showed the importance of testing the preheat temperatures, as they can have an effect on the final D_e values. They argued for conducting a preheat plateau for feldspar to determine the most appropriate preheat and measurement temperature combination for the samples, as in the case of quartz. This step seems particularly imperative in central European loess as a number of researchers have reported problems with dose recovery when applying only $pIRIR_{290}$ protocols (Schatz *et al.*, 2012; Murray *et al.*, 2014; Thiel *et al.*, 2014; Újvári *et al.*, 2014). Therefore, six preheat (205–320 °C) and elevated pIRIR temperature (25–30 °C lower than the preheat) pairings were tested. Fig. 5 shows the results of the preheat plateau conducted on sample CRO16/2/10. A plateau is observed at the three lower temperatures (205–250 °C), with an average D_e value of approximately 590 Gy. D_es increased with higher preheat temperatures (>280 °C), with the $pIRIR_{290}$ protocol producing D_e values more than twice as large (1108 ± 129 Gy, Fig. 5). This is consistent with the trends observed by both Roberts (2012) and Zhang *et al.* (2015), who also saw a tendency for D_e to increase as higher preheat temperatures were applied. Given the consistency in D_e values measured using lower temperatures, a $pIRIR_{225}$ protocol with the 250 °C preheat was selected.

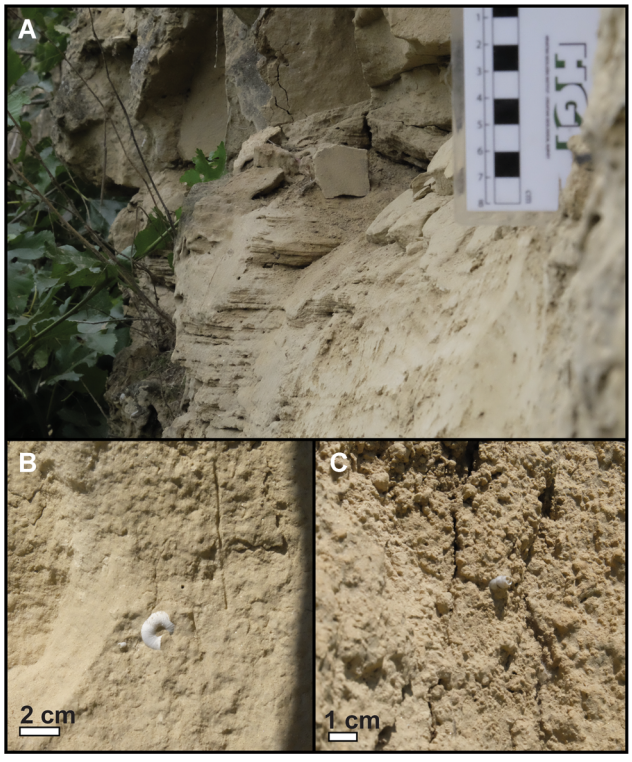

Figure 3. (A) Horizontal laminations at profile 2 (Unit VII). (B and C) Examples of gastropod shells found within Unit VI. [Color figure can be viewed at wileyonlinelibrary.com]

Dose recovery

The suitability of the selected temperature paring was tested through the dose recovery experiments, which examined the ability of the $pIRIR_{225}$ protocol to recover an administered laboratory dose. The test was applied to four samples: CRO16/2/9, CRO16/2/10, CRO16/2/17 and CRO16/2/27. Twelve aliquots per sample were used for the first three samples and six aliquots for the last sample due to sediment availability. The aliquots were bleached in daylight, irradiated in the laboratory with a beta dose approximating their natural dose and measured using the $pIRIR_{225}$ protocol (Supplementary Table S1). The average residual signal (see Residual test and signal resetting section) from the 42 discs was subtracted from the measured equivalent dose prior to calculating the dose recovery ratio. In initial dose recovery tests, the test dose constituted ~20% of the given dose, which resulted in an underestimation of the given dose by 12%. A similar trend was reported by Colarossi *et al.* (2018), who showed that low test doses (as a percentage of the given dose) supress the shape of the dose–response curve, causing D_e underestimation. To improve the performance of our SAR protocol the test dose was increased to ~30% (170 Gy) of the given dose. All discs passed the dose recovery test within uncertainty (Supplementary Figure S2). The average dose recovery ratio for $pIRIR_{225}$ protocol was 1.04 ± 0.07 ($n = 42$, Table 2).

The $2D_0$ value has been suggested as a prudent upper limit for dating (Wintle and Murray, 2006). To ensure that D_e values

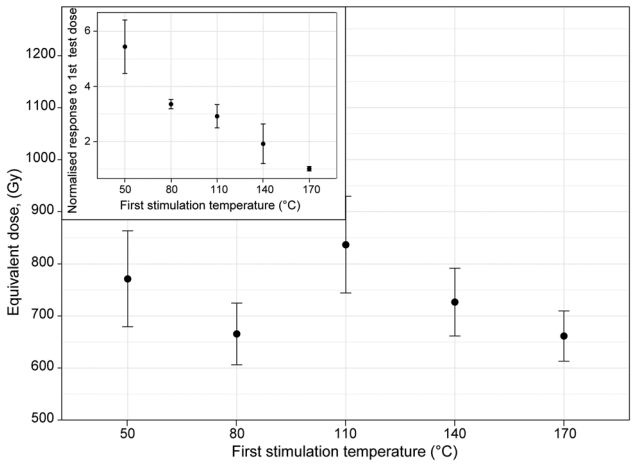

Figure 4. D_e as a function prior-IR stimulation temperature for sample CRO16/2/10. The average and standard deviation of three aliquots is shown. Inset, the $pIRIR_{225}$ response normalised to the natural test dose plotted against the first stimulation temperature.

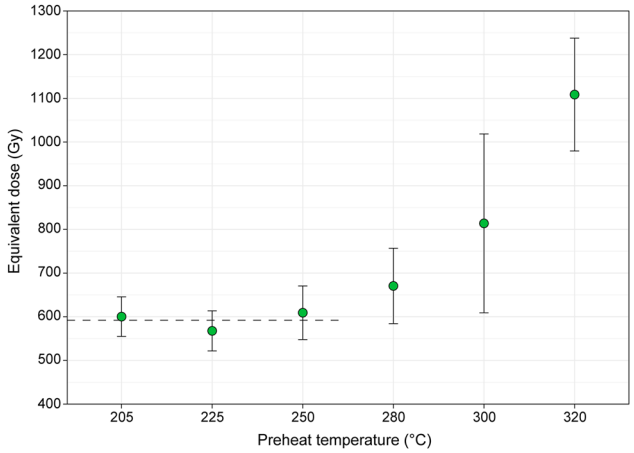

Figure 5. D_e dependency on preheat temperature for sample CRO16/2/10. The average D_e and standard deviation of three aliquots at each temperature are shown. Note the preheat plateau at lower temperature (dashed line). [Color figure can be viewed at wileyonlinelibrary.com]

used for the age calculation are not saturated, the D_0 values of each disc were checked. Fig. 6 shows a typical dose–response curve for sample CRO16/2/5, which has a $2D_0$ of 842 Gy. Taking into consideration the average dose rate at this site (3 Gy ka^{-1}), this suggests that sediment at this site can be dated to ~280 ka.

Anomalous fading

It has been suggested that all feldspars suffer from signal loss termed anomalous fading (Wintle, 1973), which can result in D_e underestimation and therefore erroneous ages. However, the pIRIR protocols have been shown to utilise more geologically stable, non-fading signal in feldspars (Thomsen *et al.*, 2008; Buylaert *et al.*, 2012). To assess the extent to which the $pIRIR_{225}$ signals from Erdut samples fade, and whether fading corrections are required (Huntley and Lamothe, 2001; Kars *et al.*, 2008) fading tests were performed. To measure the fading rates (g_{2days}) three aliquots per sample were irradiated with a fixed dose of 170 Gy repeatedly and the luminescence signal measured following a series of pauses (0, 1, 10, 100 and 1000 h) following the protocol of Auclair *et al.* (2003). Sensitivity-corrected luminescence was plotted against hold time, and data were fitted with an exponential function to determine the fading rate (%/decade normalised). The range of the fading rates for the IR_{50} signal varies between 1.14 ± 0.96%/decade and 6.91 ± 1.76%/decade (mean of 3.02 ± 1.25%/decade), whereas $pIRIR_{225}$ results range from 0.06 ± 0.85%/decade and 7.52 ± 1.81%/decade with a mean of 1.68 ± 1.13%/decade (Table 2 and Fig. 7). The results show that $pIRIR_{225}$ fades less than the IR_{50} signal. This relationship also holds true for sample CRO16/2/9 for which the average $pIRIR_{225}$ fading rate is slightly higher than the other samples (3.30 ± 1.37%/decade). The fading rate for this sample is a result of an unusually high fading rate recorded for one aliquot, 7.52 ± 1.81%/decade (Fig. 7), which increases the average fading result for this sample. Out of the remaining two aliquots, one is found within the accepted fading range for the pIRIR protocol (0.09 ± 0.86%/decade), while the other one is only borderline (2.29 ± 1.43%/decade). Given the generally low fading rates calculated, fading correction was not applied to the majority of the samples as the recorded $pIRIR_{225}$ fading is in line with previously reported laboratory fading rates for non-fading quartz signals (Buylaert *et al.*, 2012). Nonetheless, as sample CRO16/2/9 was found to be borderline acceptable, the age was corrected for fading and presented alongside the uncorrected age. The correction was performed in the R Luminescence package using the calc_FadingCorr script (Kreutzer, 2019) which is based on the Huntley and Lamothe (2001) calculation.

Residual test and signal resetting

Sunlight exposure during aeolian transport should almost completely bleach signal in feldspar (Buylaert *et al.*, 2011). Nonetheless, testing for the size of the residual component is important in aeolian samples because feldspars may have an unbleachable 'residual' component which, if large enough, could cause age overestimation (Stevens *et al.*, 2011). Sets of 6–12 aliquots from samples CRO16/2/9, CRO16/2/10,

Table 2. Results of the residual, dose recovery and fading tests carried out on selected samples. All data are shown with 1 σ errors. *Residual subtracted dose recovery ratio.

	Potassium feldspars			
Sample	Residual dose (Gy)	Dose recovery*	IR_{50} g-value (%)	$pIRIR_{225}$ g-value (%)
CRO16/2/15	–	–	3.23 ± 1.22	0.31 ± 0.88
CRO16/2/9	6.31 ± 0.27	1.07 ± 0.09	4.66 ± 1.53	3.30 ± 1.37
CRO16/2/10	4.60 ± 0.18	1.05 ± 0.08	2.82 ± 1.26	1.62 ± 1.12
CRO16/2/15	–	–	3.18 ± 1.19	1.55 ± 1.19
CRO16/2/17	4.11 ± 0.16	1.04 ± 0.07	2.41 ± 1.13	1.90 ± 1.14
CRO16/2/21	–	–	1.79 ± 1.20	1.38 ± 1.09
CRO16/2/27	4.37 ± 0.17	0.98 ± 0.07	–	–
Average	$\mathbf{4.71 \pm 0.19}$	$\mathbf{1.04 \pm 0.07}$	$\mathbf{3.02 \pm 1.25}$	$\mathbf{1.68 \pm 1.13}$

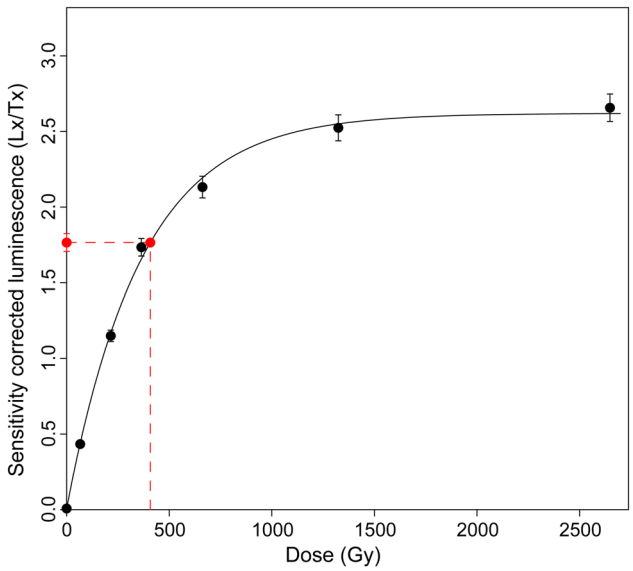

Figure 6. The $pIRIR_{225}$ dose–response curve from an aliquot of CRO16/2/5. The natural signal is shown by the red circle and dashed red line. [Color figure can be viewed at wileyonlinelibrary.com]

CRO16/2/17 and CRO16/2/27 were bleached in daylight for 10 days (in May in the UK). Samples were then measured using the same $pIRIR_{225}$ protocol to determine the residual signal remaining after bleaching. The average residual component in all measured samples is 4.71 ± 0.19 Gy (3.38–6.81 Gy range; Table 2), which is relatively small in comparison with some reported European loess studies. Thiel *et al.* (2011a), for example, presented a 15–20 Gy unbleachable component in Austrian loess, and Stevens *et al.* (2011) found residuals as high as 40 Gy in Serbian loess.

Given that the IR signals are much harder to bleach in nature than quartz (Godfrey-Smith *et al.*, 1988), samples were further investigated to eliminate the possibility that the signals were not fully reset prior to the burial. To test this, IR_{50} signals, which bleach more rapidly in nature, were compared with pIRIR signals (Supplementary Fig. S3). Fading corrected IR_{50} ages are slightly lower than $pIRIR_{225}$ ages, with an average ratio between the two of 0.86 ± 0.09 σ, although if the individual ratio of 0.58 for sample CRO16/2/25 is excluded, the overall ratio increases to

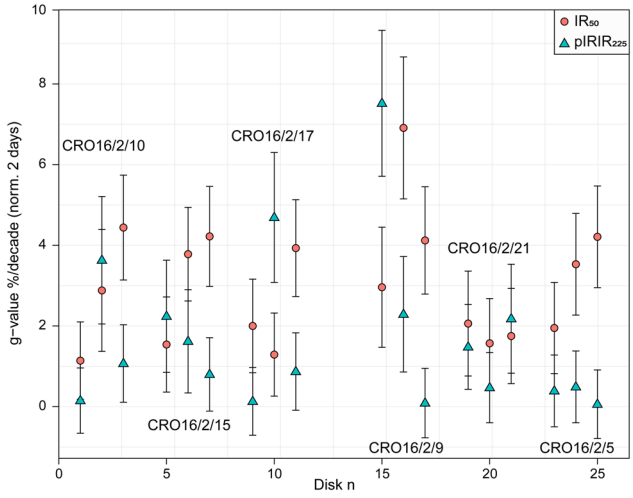

Figure 7. Calculated fading rates for the IR_{50} and $pIRIR_{225}$ luminescence signals for all measured samples (three discs per sample). All data are shown with 1 σ errors. [Color figure can be viewed at wileyonlinelibrary.com]

0.89 ± 0.04 σ. Given that in all cases the IR_{50} fading correction is applied to relatively old ages, and therefore the non-linear portion of the dose–response curve these results were accepted as indicative of reasonable signal resetting of both the IR_{50} and $pIRIR_{225}$ signals. For sample CRO16/2/25 the underestimation is much greater (~58%), which could suggest that the signal was not fully reset in nature and therefore the age of this sample may be overestimated. However, the age is stratigraphically consistent with the samples above and below, and therefore is accepted.

D_e calculation

Luminescence signals were screened using typical rejection criteria, i.e. signal recuperation (<5% of the natural), and recycling ratios of 1 ± 10% (Murray and Wintle, 2000). For all measured signals (n = 193), all discs passed the recycling ratio (1.03 ± 0.05), and recuperation was less than 0.57 ± 0.03%. Overdispersion values recorded varied between 0 and 6.7%, with the majority of samples recording no overdispersion. Therefore, equivalent doses were calculated by applying the Central Age Model (Galbraith *et al.*, 1999).

Age–depth model and mass accumulation rates

To assist with the investigation of the age change with depth, and calculation of accumulation rates, an age–depth model based on the $pIRIR_{225}$ ages was constructed using Zeeden *et al.* (2018) R package. It uses Bayesian and inverse modelling to separate systematic and random errors of luminescence age by creating probability density functions for both, and include only the latter in the uncertainty calculations. All ages discussed in the text refer to modelled ages (Supplementary Table S2).

To investigate dust fluxes and interpret sedimentary deposition, mass accumulation rates (MARs) were calculated based on modelled luminescence ages, following the equation of Kohfeld and Harrison (2003):

$$\mathrm{MAR}(\mathrm{g m^{-2} a^{-1}}) = \mathrm{SR} \times f_{eol} \times \rho_{\mathrm{dry}} \quad (1)$$

where, SR denotes the sedimentation rate (m a^{-1}), f_{eol} is the fraction of the sediment that is aeolian in origin, and ρ_{dry} represents the bulk density of dry sediment (g m^{-3}). The sediment was interpreted to be aeolian in origin, therefore a f_{eol} value of 1 was used. The commonly applied loess bulk density value of 1.5 g cm^{-3} (Újvári *et al.*, 2010; Perić *et al.*, 2019) was used. Minimum and mean MARs were calculated based on a minimum and mean sedimentation following the suggestion of Leighton *et al.* (2014).

Results and discussion

A new chronology for the Erdut loess–palaeosol section

Thirteen unmodelled and modelled $pIRIR_{225}$ luminescence ages from Units V to IX are presented in Figs 8 and 9, Table 3 and Supplementary Table S2. The top of Unit IV was dated to 75.01 ± 5.44 ka. Five ages were measured from the underlying thick loess, Unit VI. The uppermost sample, collected at the Erdut 3 profile, 40 cm below the palaeosol–loess boundary provided an age of 139.18 ± 8.75 ka. The remaining three ages from both Erdut 3 and 4 are quite closely spaced at 140.48 ± 7.52 ka, 143.29 ± 7.76 ka and 145.47 ± 9.33 ka. While the bottom sample from the Erdut 4 profile was dated to 170.14 ± 13.49 ka. This could indicate a sediment gap contained in a metre of sediment; however, the size and the exact position of this hiatus requires further investigation.

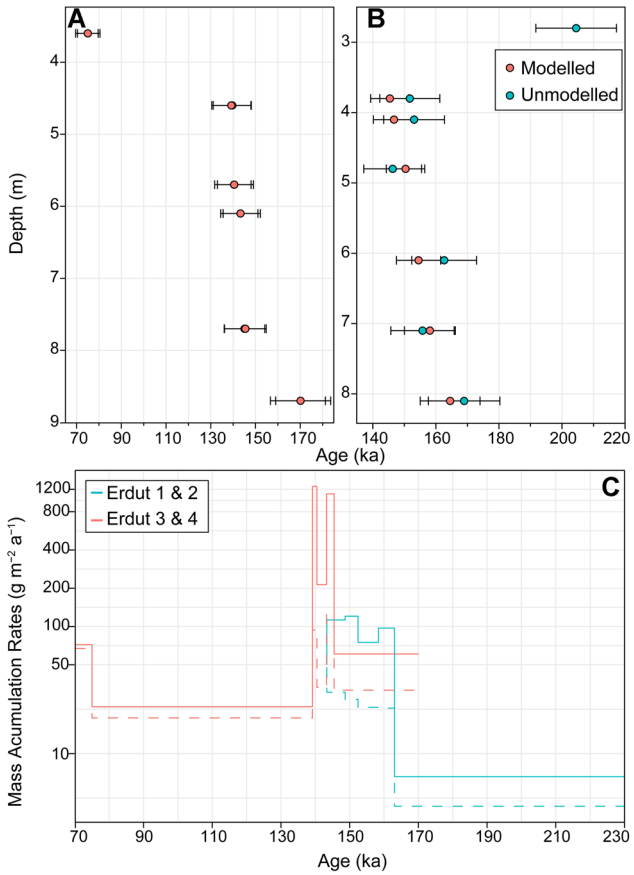

Figure 8. A comparison of the modelled and unmodelled pIRIR$_{225}$ ages for Erdut profiles (A) 3 and 4 and (B) 1 and 2. Please note that the top age in 9B (CRO16/2/10) is only presented as an unmodelled value as it is an outlier. (C) Mass accumulation rates (g m^2 a^{-1}) for Erdut presented as mean (solid line) and minimum (dashed values) values based on the modelled ages. [Color figure can be viewed at wileyonlinelibrary.com]

Ages from profiles 3 and 4 differ markedly from those in the chronology of Galović *et al.* (2009). Based on the stratigraphic position it is likely that one of the ages presented by Galović *et al.* (2009), 53.8 ± 5.4 ka, corresponds to Unit VI. However, it is not possible to establish the relationship between the depth of their samples and the depths of the samples presented here. Therefore, while underestimation is observed, there are a number of factors that could be contributing to this discrepancy, including, for example, use of an uncorrected IR$_{50}$ signal for the equivalent dose estimation (Galović *et al.*, 2009) or use of different grain size fractions (63–90 μm potassium feldspar herevs 4–11 μm polymineral (Galović *et al.*, 2009)) between two studies. The uncorrected IR$_{50}$ ages (Supplementary Table S3) for Unit VI show ages in a similar range (53.19–98.96 ka) to those reported by Galović *et al.* (2009). This suggests that the use of uncorrected IR$_{50}$ signal for the equivalent dose estimation is probably the largest source of age underestimation. However, this requires further investigation and is beyond the scope of this paper. Galović *et al.* (2009) did not obtain ages from the palaeosol (Unit V); however, they attributed ages 46.9 ± 4.8 and 46.5 ± 4.7 ka to the loess above it. While these ages cannot be verified, in view of the rest of the chronological results, they are likely to be underestimated.

At profiles 1 and 2 the luminescence ages provide chronology for laminated sediment (Unit VII), loess (Unit VIII) and bottom palaeosol (Unit IX). Sample CRO16/2/10 (203.73 ± 12.8 ka) from the top of the laminated unit, appears to be significantly overestimating the depositional age and is the only age inconsistent with the rest of the chronological record (within uncertainties). Based on stratigraphy, field observations and grain size analysis (Figs 2 and 3 and Table 1), this sample is interpreted as fluvial in origin. Therefore, a ~60 ka age reversal could potentially be explained by incomplete bleaching of the sediment. Partial bleaching is not unusual in fluvial sediments as complete exposure to light may be restricted in sediment-lain water (Wallinga, 2002). However, it is unclear why the discrepancy is recorded only in one sample and without further investigation using single grain approaches it is difficult to interpret this age.

Four ages from the lowest loess unit (VIII), at Erdut 1 and 2, fall in the 148.69 ± 6.98–158.42 ± 7.77 ka age range, covering a period of 10–16 ka (based on mean and minimum ages). As with Unit VI it is not possible to correlate more precisely the depth at which Galović *et al.* (2009) sampled from this Unit, and therefore compare it with the results of this study. Nonetheless, their results provide an uncorrected IR$_{50}$ age of 61.5 ± 6.2 ka which corresponds to 85 ± 5.6–92.9 ± 6.2 ka IR$_{50}$ age range (Supplementary Table S3). As highlighted above, there are other potential sources of the discrepancy, including mineral fraction and grain size, though the largest

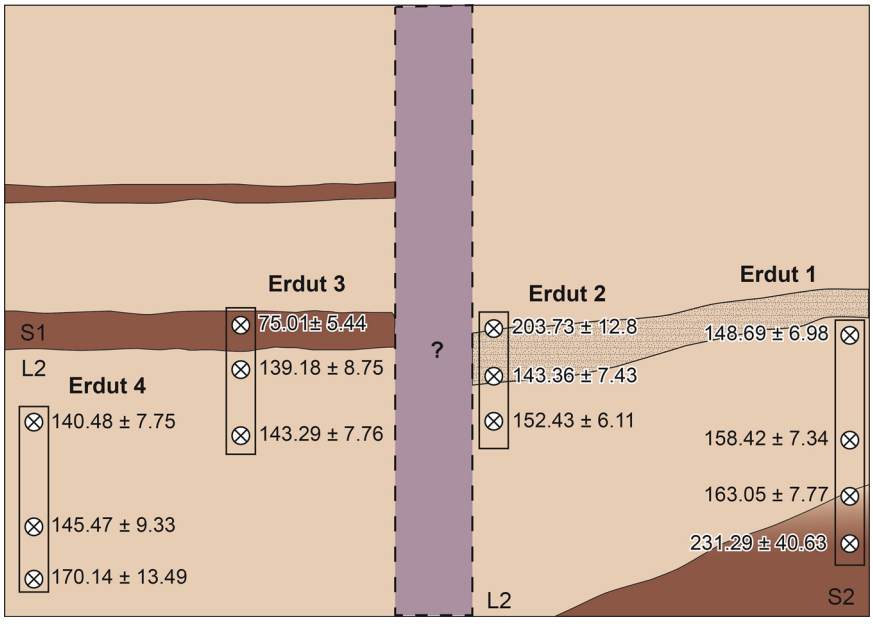

Figure 9. A schematic stratigraphy diagram for the four profiles at Erdut with modelled luminescence ages shown. The blue rectangle marks the area of stratigraphical uncertainty. [Color figure can be viewed at wileyonlinelibrary.com]

Table 3. Samples, depths, radionuclide concentrations, dose rates, D_e values and the final luminescence ages obtained using the $pIRIR_{225}$ protocol applied to 63–90 μm potassium feldspars. In bold are highlighted ages used for modelling. *m – measured, a – accepted; **Overdispersion; ***Corrected pIRIR225.

Sample	Depth (m)	Unit	U (ppm ± 1σ)	Th (ppm ± 1σ)	Rb (ppm ± 1σ)	K (% ± 1σ)	Cosmic dose rate (Gy/ka)	Total dose rate (Gy/ka)	Aliquots (m/a)*	OD (%)**	D_e (Gy)	Uncorrected $pIRIR_{225}$ age (ka)
						PROFILE 1						
CRO16/2/1	4.1	VIII	1.95 ± 0.19	9.79 ± 0.98	79.74 ± 7.97	1.62 ± 0.16	0.13 ± 0.01	3.18 ± 0.19	15/15	2.5	484.55 ± 9.57	**152.58 ± 9.58**
CRO16/2/5	6.1	VIII	1.80 ± 0.18	9.21 ± 0.92	83.28 ± 8.33	1.67 ± 0.17	0.10 ± 0.01	3.11 ± 0.19	15/15	0	500.96 ± 9.15	**162.01 ± 10.22**
CRO16/2/7	7.1	IX	1.97 ± .020	10.73 ± 1.07	89.97 ± 9.00	1.79 ± 0.18	0.09 ± 0.01	3.38 ± 0.21	15/15	2.3	521.80 ± 11.0	**154.48 ± 9.92**
CRO16/2/9	8.1	IX	2.02 ± 0.20	11.69 ± 1.17	101.08 ± 10.1	1.86 ± 0.19	0.09 ± 0.01	3.52 ± 0.22	13/13	0	592.40 ± 16.2	168.37 ± 11.27 **233.99 ± 49.69*****
						PROFILE 2						
CRO16/2/10	2.8	VII	1.88 ± 0.19	10.55 ± 1.06	59.99 ± 6.00	1.24 ± 0.12	0.15 ± 0.02	2.91 ± 0.17	15/15	8.7	592.28 ± 12.1	**203.73 ± 12.80**
CRO16/2/12	3.8	VII	1.89 ± 0.19	10.06 ± 1.01	84.57 ± 8.46	1.77 ± 0.18	0.13 ± 0.01	3.32 ± 0.20	15/15	0	501.82 ± 9.0	**151.27 ± 9.47**
CRO16/2/14	7.8	VIII	1.99 ± 0.20	10.42 ± 1.04	81.66 ± 8.17	1.67 ± 0.17	0.12 ± 0.01	3.27 ± 020	15/15	0	477.21 ± 8.4	**145.81 ± 9.11**
						PROFILE 3						
CRO16/2/15	3.6	V	2.00 ± 0.20	10.05 ± 1.01	84.85 ± 8.48	1.82 ± 0.18	0.14 ± 0.01	3.40 ± 0.20	15/15	6.8	254.77 ± 3.9	**75.01 ± 4.67**
CRO16/2/17	4.6	VI	1.75 ± 0.17	7.95 ± 0.79	60.48 ± 6.05	1.37 ± 0.14	0.13 ± 0.01	2.74 ± 0.16	15/15	8.3	382.80 ± 6.1	**139.61 ± 8.54**
CRO16/2/20	6.1	VI	1.87 ± 0.19	8.44 ± 0.84	67.44 ± 6.74	1.54 ± 0.15	0.10 ± 0.01	2.94 ± 0.18	15/15	6.3	413.00 ± 6.4	**140.42 ± 8.66**
						PROFILE 4						
CRO16/2/21	5.7	VI	1.84 ± 0.18	8.43 ± 0.84	65.31 ± 6.53	1.51 ± 0.15	0.11 ± 0.01	2.92 ± 0.17	15/15	0	418.46 ± 6.9	**143.29 ± 8.86**
CRO16/2/25	7.7	VI	1.64 ± 0.16	8.39 ± 0.84	68.30 ± 6.83	1.56 ± 0.15	0.09 ± 0.01	2.88 ± 0.17	15/15	0	422.27 ± 7.63	**145.08 ± 9.09**
CRO16/2/27	8.7	VI	1.91 ± 0.19	9.57 ± 0.96	71.44 ± 7.14	1.54 ± 0.15	0.08 ± 0.01	3.03 ± 0.18	15/15	6.7	515.5 ± 13.0	**170.14 ± 11.13**

driver appears to be the use of uncorrected IR_{50} signal. The Erdut 1 profile culminates in a thick palaeosol (Unit IX), dated to 231.29 ± 40.63 ka (uncorrected 168.37 ± 11.27 ka). These results suggest that this section spans two glacial–interglacial cycles, rather than just one as was previously proposed.

Despite a large overlap between ages from two parts of the profile (Figs 8 and 9), the lateral disappearance of the palaeosols and the laminated fluvial sediments prevents this record from being consolidated into one. Further, the chronological gap recorded at the bottom of profile 4 requires further attention.

Mass accumulation rates

High-resolution loess chronologies extending beyond the penultimate interglacial are limited. As a result, so are mass accumulation rates for this period. Fig. 8C shows the MARs based on the modelled $pIRIR_{225}$ ages for the Erdut outcrop. While the most commonly taken approach relies on calculation of MARs based on only the mean age, it has been shown that in an aeolian context this may lead to misleading interpretations of luminescence ages (Leighton *et al.*, 2014). Therefore, the results presented here also show the minimum MAR values.

Palaeosol Unit IX records the lowest accumulation rate in the whole section: 6 g m^{-2} a^{-1} and 4 g m^{-2} a^{-1}, mean and minimum respectively, though Unit V's rates are also low (19–23 g m^{-2} a^{-1}). Conversely, rates within loess are not only high but also quite variable. The top part of the loess Unit VI shows very rapid accumulation 94–1265 g m^{-2} a^{-1}. However, between 143 and 140 ka MARs drop to the average 213 g m^{-2} a^{-1} (minimum 33 g m^{-2} a^{-1}). These shifts could indicate changes in a number of factors including sediment production at source, sediment transport (either by the Danube River or the wind), preservation potential, wind direction, and activation/deactivation of an additional or new source.

Importantly, Fig. 8 shows that loess deposition has been neither uniform nor continuous, which are common assumptions in loess research. By nature, loess is a very homogeneous sediment in which depositional gaps or erosional events are not obvious when assessing the stratigraphy. Furthermore, the homogeneity also means that even if an erosional event did occur, the new sediment is likely to have a similar grain size and magnetic susceptibility to the one deposited before. Therefore, unless a change in source or material delivered to a site occurred as well, hiatuses will be difficult to identify from the proxy record. At Erdut the erosional gap is represented by fluvial sediments in profiles 1 and 2. However, fluvial sediments are not preserved in profile 4, yet the dates suggest a sedimentary gap. This hiatus should be further investigated as its size may vary between 1.85 and 47.5 ka, depending on whether a minimum or maximum error is used.

With more high-resolution dating studies conducted, the size of hiatuses in loess records could be better constrained and investigated in the context of climatic and/or local influences on the loess deposition. Whether climatically or locally driven, a number of gaps in loess records have been reported at multiple locations (e.g. Dong *et al.*, 2015; Stevens *et al.*, 2018), highlighting the danger of the loess continuity assumption. The profiles at Erdut provide a unique view of the issue as profile 4 shows a hiatus that would not be recognised due to the lack of lithological changes. However, 100 m away profiles 1 and 2 preserve the likely cause of the gap. This not only shows a need for high-resolution chronological approaches but also investigation of sedimentological sections in a wider spatial context.

Environmental implications

Samples CRO16/2/9 and CRO16/2/7, from the middle of the gradational boundary and the top of Unit IX at Erdut, provide modelled ages of 231.29 ± 40.63 ka and 163.05 ± 7.77 ka, respectively (Fig. 9). This thick, dark and well-developed palaeosol reportedly has relatively high total organic carbon (TOC) content and a large proportion of clay and fine silts (Galović *et al.*, 2009). Although the corrected age for the palaeosol has a very large uncertainty, it falls well within the bounds of MIS 7 and is therefore identified as S2 soil. The luminescence age from the stratigraphic boundary between loess and palaeosol likely represents the transition period between MIS 6 and MIS 7 stages. Other detailed and dated climatic archives for this period are scarce, with the majority located near the southern Balkans and Mediterranean Sea.

As only the transitional zone and top of this palaeosol is exposed, it is not possible to determine the full thickness and appearance of Unit IX palaeosol in Erdut. In the Danubian loess, S2 is represented as a double or triple palaeosol pedocomplex with a strongly developed S2S1 palaeosol that has enhanced magnetic susceptibility values (Marković *et al.*, 2006, 2009; Buggle *et al.*, 2009; Wacha *et al.*, 2013). Currently it is not possible to determine how many palaeosols are preserved at Erdut and therefore how this site fits into the regional loess stratigraphy.

Based on the modelled luminescence ages, Units VIII and VI likely represent the same period of loess deposition (Fig. 9). However, at present it is impossible to precisely combine them into a single stratigraphic unit. Loess accumulation at Erdut began at 170.14 ± 13.49 ka and concluded soon after 139.18 ± 8.75 ka, showing that the site experienced semi-continuous loess deposition for 9–53 ka, based on minimum and maximum ages, respectively (Fig. 9). The chronology suggests that these Units provide a record of MIS 6 and are therefore classified as L2 loess. Further, a drop in the TOC associated with decreased biological productivity, as well as an increase in the proportion of coarse silt and sand is noted in this unit (Galović *et al.*, 2009). These changes suggest increased windiness and/or a change in wind direction, a change in sediment supply, or new source activation; all likely possibilities during glacial periods.

The sites extending beyond the last interglacial are often located near the Danube (Fig. 1). Along the Danube the L2 loess is not as well preserved or exposed as the L1 (the record of the last glacial period). In many cases just the top of the L2 unit is exposed at the base of profiles (*cf* Fitzsimmons *et al.*, 2012). Nonetheless, the thickness of the exposed L2 unit at Erdut, Vukovar (Wacha and Frechen, 2011), Ruma (Marković *et al.*, 2006), Batajnica (Marković *et al.*, 2009), Süttő (Novothny *et al.*, 2011), Costinești (Constantin *et al.*, 2014) and Harletz (Lomax *et al.*, 2018), indicates large quantities of sediment available for transport and deposition along the Danube corridor. This is not surprising as the MIS 6 stage is considered to be one of the most climatically severe periods in Europe, with the farthest extent of the glaciers (Ehlers and Gibbard, 2007; Francke *et al.*, 2016). The glacial action producing the sediment, increased fluvial and aeolian transport, in combination with a cold and dry climate and predominantly dry steppe and/or forest steppe-like conditions (Marković *et al.*, 2006, 2007, 2018) supports increased sediment availability in the system.

Fig. 8 shows that this period is marked by highly variable accumulation rates. All Erdut's profiles indicate that in the early parts of MIS 6, rates were relatively low: 32–60 g m^{-2} a^{-1} (Erdut 1 and 2) and 23–97 g m^{-2} a^{-1} (Erdut 3 and 4). This is followed by a temporary drop to 75 g m^{-2} a^{-1} (mean) between 158.42 ± 7.34 and

152.43 ± 6.11 ka and rise to ~120 g m^{-2} a^{-1} (mean). At Erdut 1 and 2, rates increase rapidly (mean 1104 g m^{-2} a^{-1} and 125 g m^{-2} a^{-1}) after 145.47 ± 9.33 ka, drop to 213 g m^{-2} a^{-1} (mean) at 143.29 ± 7.76 ka, and increase to their highest mean value (1265 g m^{-2} a^{-1}; minimum 94 g m^{-2} a^{-1}) between 140.48 ± 7.52 and 139.18 ± 8.75 ka, after which the rates drop until the beginning of MIS 5. This further supports the suggestion that MIS 6 can be divided into two parts at around 155 ka (Margari *et al.*, 2010), with the first part resembling more of an interstadial, and the full glacial conditions beginning after 155 ka, as the global ice volume increases to reach glacial maximum. The division at Erdut is seen in both minimum and mean MARs and occurs after ~152 ka in agreement with Margari *et al.* (2010). This again highlights that loess accumulation is not uniform and continuous during glacial periods and suggests that the sediment dynamics were highly susceptible to change and continued to respond to climatic and/or geomorphological changes.

At the profiles closest to the modern river channel (Erdut1 and 2), the L2 is punctuated by a series of horizontally and cross-laminated sand and silt. These are absent from profiles 3 and 4, only 100 m further away. Laminated deposits were previously interpreted as fluvial (Galović *et al.*, 2009; Galović, 2014), which is supported by field observations conducted during this research. The deposition of Unit VII commenced between 148.69 ± 6.98 ka and 143.36 ± 7.43 ka. However, its termination is unclear as the unmodelled luminescence age from the top of the unit dates it to 203.73 ± 12.8 ka. This age is not consistent with the rest of the stratigraphic and chronological record at Erdut and is probably an overestimation based on the sample's stratigraphic position (see discussion in A new chronology for the Erdut loess-palaeosol section). While profiles 3 and 4 do not contain laminated sediments, a hiatus in ages (170.14 ± 13.49–145.47 ± 9.33 ka), corresponding to the onset of fluvial sediment, suggests that the whole site may have been subject to fluvial influence.

This temporary shift to fluvial sedimentation could indicate changes to the Danube's main channel or a development of a small branching channel. Fluvial sediments also punctuate the L2 unit at Stari Slankamen (Marković *et al.*, 2011) and Zmajevac (Galović *et al.*, 2009; Banak *et al.*, 2012) either as a series of laminated sediments or as an erosional feature. Further fluvial features at Šarengrad (Galović *et al.*, 2009) could also be of the same age. However, this cannot be confirmed until the chronologies for these sections are verified and more detailed sedimentological investigations are conducted. Nonetheless, this could indicate a basin-wide hydrological event, potentially restricted to the sites found along the main Danube corridor. However, the exact timing and cause of this event cannot be resolved due to the uncertainty on luminescence dates.

The relatively thin palaeosol (Unit V) dates to 75.01 ± 5.44 ka, with the loess sample below providing a bracketing age of 139.18 ± 8.75 ka, suggesting that this palaeosol represents the last interglacial (MIS 5) (Rasmussen *et al.*, 2014). The bottom age estimate is in line with the onset of Termination II (Moseley *et al.*, 2015), the transition from MIS 6 into MIS 5, supporting its identification as the last interglacial soil (S1).This is also supported by an increase in clay particles and TOC to the highest values in the section (Galović *et al.*, 2009). It is possible that Erdut experienced locally driven, favourable conditions for the pedogenesis to occur over ~50 ka (Fig. 9), that resulted in low MARs (Fig. 8). Therefore, Unit V could be preserving a record of the whole interglacial period, including all of the substages in a single palaeosol.

However, the S1 palaeosol at Erdut is relatively thin in comparison with palaeosols of that age across the region (*cf* Fitzsimmons *et al.*, 2012), e.g. the three-times thicker S1 palaeosol at Vukovar (Wacha and Frechen, 2011), a few kilometres downstream. Furthermore, other S1 palaeosols in the Carpathian Basin, e.g. Dunaszekcső (Újvári *et al.*, 2014), Süttő (Novothny *et al.*, 2011) and Dolní Věstonice (Fuchs *et al.*, 2013) are represented by double or triple palaeosols. Consequently, partial erosion of the other the pedocomplex at Erdut is likely.

Nevertheless, S1 pedogenic complexes are heterogeneous across the region (*cf* Fitzsimmons *et al.*, 2012), and palaeosols at Erdut could reflect pedogenic processes driven by local conditions such as palaeotopography (including drainage), vegetation, proximity to the river, and micro-climate (Vandenberghe *et al.*, 2014; Lehmkuhl *et al.*, 2016). This could be pointing to regional and/or local drivers preserved in the loess records on the sub-orbital level. Therefore, the S1 palaeosol at Erdut requires further high-resolution chronological analysis combined with a detailed sedimentological and micromorphological investigation.

Conclusions

A review of the chronology for the loess–palaeosol sequence at Erdut is presented, based on coarse-grain (63–90 μm) potassium feldspar and a pIRIR$_{225}$ measurement protocol. The modelled uncorrected pIRIR$_{225}$ ages range from 75.01 ± 5.44 to 231.29 ± 40.63 ka, which suggest a semi-continuous loess accumulation at this site since MIS 7. The results show that Erdut preserves much longer climatic and environmental records than originally thought and could therefore greatly contribute to our understanding of the long-term Pleistocene changes in the region. A fluvial event, which disturbed L2 loess accumulation, is also reported. This could be pointing to a wider hydrological that affected loess deposits along the main Danube channel (e.g. Stari Slankamen (Murray *et al.*, 2014)). Other sites in Croatia (Zmajevac and Šarengrad) that preserve fluvial sedimentary sequences in L2 were dated using an uncorrected IR$_{50}$ protocol, which this research shows is likely to be underestimating ages. Therefore, it is not possible to compare and provide a more detailed picture of the fluvial event. Consequently, chronologies at Zmajevac and Šarengrad should be revisited. Finally, this research shows that more high-resolution approaches based on the pIRIR protocols are needed to better understand the timing of the climatic and environmental changes during the penultimate glacial–interglacial stage.

Supporting information

Additional supporting information may be found in the online version of this article at the publisher's web-site.

Supporting information.

Acknowledgements. This research was funded by the UK Natural Environmental Research Council (grant: NE/L002612/1), International Association of Sedimentologists Postgraduate Research Grant, and Hertford College Travel Fund. We are grateful to two anonymous reviewers for their constructive comments.

References

An Z. 2000. The history and variability of the East Asian paleomonsoon climate. *Quaternary Science Reviews* **19**: 171–187.

Antoine P, Rousseau D-D, Fuchs M *et al.* 2009. High-resolution record of the last climatic cycle in the southern Carpathian Basin (Surduk, Vojvodina, Serbia). *Quaternary International* **198**: 19–36.

Auclair M, Lamothe M, Huot S. 2003. Measurement of anomalous fading for feldspar IRSL using SAR. *Radiation Measurements* **37**: 487–492.

Balescu S, Lamothe M. 1994. Comparison of TL and IRSL age estimates of feldspar coarse grains from waterlain sediments. *Quaternary Geochronology* **13**: 437–444.

Balescu S, Lamothe M, Panaiotu C *et al.* 2010. IRSL chronology of eastern Romanian loess sequences. *Quaternaire* **21**: 115–126.

Banak A, Mandic O, Kovačić M *et al.* 2012. Late Pleistocene climate history of the Baranja loess plateau – evidence from the Zmajevac loess-paleosol section (northeastern Croatia). *Geologia Croatica* **65**: 411–422.

Brennan BJ, Lyons RG, Phillips SW. 1991. Attenuation of alpha particle track dose for spherical grains. *International Journal of Radiation Applications and Instrumentation* **18**: 249–253.

Buggle B, Hambach U, Glaser B *et al.* 2009. Stratigraphy, and spatial and temporal paleoclimatic trends in Southeastern/Eastern European loess–paleosol sequences. *Quaternary International* **196**: 86–106.

Buylaert J-P, Thiel C, Murray AS *et al.* 2011. IRSL and post-IR IRSL residual doses recorded in modern dust samples from the Chinese Loess Plateau. *Geochronometria* **38**: 432–440.

Buylaert J-P, Jain M, Murray AS *et al.* 2012. A robust feldspar luminescence dating method for Middle and Late Pleistocene sediments. *Boreas* **41**: 435–451.

Colarossi D, Duller GAT, Roberts HM. 2018. Exploring the behaviour of luminescence signals from feldspars: Implications for the single aliquot regenerative dose protocol. *Radiation Measurements* **109**: 35–44.

Constantin D, Begy R, Vasiliniuc S *et al.* 2014. High-resolution OSL dating of the Costineşti section (Dobrogea, SE Romania) using fine and coarse quartz. *Quaternary International* **334–335**: 20–29.

Dong Y, Wu N, Li F *et al.* 2015. Time-transgressive nature of the magnetic susceptibility record across the Chinese Loess Plateau at the Pleistocene/Holocene transition. *PLoS ONE* **10**: 1–16.

Durcan JA, King GE, Duller GAT. 2015. DRAC: Dose Rate and Age Calculator for trapped charge dating. *Quaternary Geochronology* **28**: 54–61.

Ehlers J, Gibbard PL. 2007. The extent and chronology of Cenozoic Global Glaciation. *Quaternary International* **164–165**: 6–20.

Fitzsimmons KE, Marković SB, Hambach U. 2012. Pleistocene environmental dynamics recorded in the loess of the middle and lower Danube basin. *Quaternary Science Reviews* **41**: 104–118.

Francke A, Wagner B, Just J *et al.* 2016. Sedimentological processes and environmental variability at Lake Ohrid (Macedonia, Albania) between 637 ka and the present. *Biogeosciences* **13**: 1179–1196.

Fuchs M, Kreutzer S, Rousseau D-D *et al.* 2013. The loess sequence of Dolní Věstonice, Czech Republic: A new OSL-based chronology of the Last Climatic Cycle. *Boreas* **42**: 664–677.

Galbraith RF, Roberts RG, Laslett GM *et al.* 1999. Optical Dating of Single and Multiple Grains of Quartz From Jinmium Rock Shelter, Northern Australia: Part I, Experimental Design and Statistical Models. *Archaeometry* **41**: 365–395.

Galović L. 2014. Geochemical archive in the three loess/paleosol sections in the Eastern Croatia: Zmajevac I, Zmajevac and Erdut. *Aeolian. Research* **15**: 113–132.

Galović L, Frechen M, Halamić J *et al.* 2009. Loess chronostratigraphy in Eastern Croatia-A luminescence dating approach. *Quaternary International* **198**: 85–97.

Godfrey-Smith DI, Huntley DJ, Chen WH. 1988. Optical dating studies of quartz and feldspar sediment extracts. *Quaternary Science Reviews* **7**: 373–380.

Guérin G, Mercier N, Adamiec G. 2011. *Dose-rate conversion factors: update. Ancient TL* **29**: 5–8.

Huntley DJ, Baril MR. 1997. The K content of the K-feldspars being measured in optical dating or in thermoluminescence dating. *Ancient TL* **15**: 11–13.

Huntley DJ, Lamothe M. 2001. Ubiquity of anomalous fading in K-feldspars and the measurement and correction for it in optical dating. *Canadian Journal of Earth Sciences* **38**: 1093–1106.

Jain M, Ankjærgaard C. 2011. Towards a non-fading signal in feldspar: Insight into charge transport and tunnelling from time-resolved optically stimulated luminescence. *Radiation Measurements* **46**: 292–309.

Jordanova D, Hus J, Evlogiev J *et al.* 2008. Palaeomagnetism of the loess/palaeosol sequence in Viatovo (NE Bulgaria) in the Danube basin. *Physics of the Earth and Planetary Interiors* **167**: 71–83.

Kars RH, Wallinga J, Cohen KM. 2008. A new approach towards anomalous fading correction for feldspar IRSL dating - tests on samples in field saturation. *Radiation Measurements* **43**: 786–790.

Kohfeld KE, Harrison SP. 2003. Glacial-interglacial changes in dust deposition on the Chinese Loess Plateau. *Quaternary Science Reviews* **22**: 1859–1878.

Kreutzer S 2019. calc_FadingCorr(): Apply a fading correction according to Huntley & Lamothe (2001) for a given g-value and a given tc. Function version 0.4.2. In *Luminescence: Comprehensive Luminescence Dating Data AnalysisR package version 0.9.5*, Kreutzer S, Burow C, Dietze M, *et al.* (eds).

Kukla GJ. 1977. Pleistocene land-sea correlations I. *Europe. Earth Science Reviews* **13**: 307–374.

Lacey JH, Leng MJ, Francke A *et al.* 2016. Mediterranean climate since the Middle Pleistocene: A 640 ka stable isotope record from Lake Ohrid (Albania/Macedonia). *Biogeosciences Discussions* **12**: 13427–13481.

Lamothe M, Auclair M. 1999. A solution to anomalous fading and age shortfalls in optical dating of feldspar minerals. *Earth and Planetary Science Letters* **171**: 319–323.

Lehmkuhl F, Zens J, Krauß L *et al.* 2016. Loess-paleosol sequences at the northern European loess belt in Germany: Distribution, geomorphology and stratigraphy. *Quaternary Science Reviews* **153**: 11–30.

Leighton CL, Thomas DSG, Bailey RM. 2014. Reproducibility and utility of dune luminescence chronologies. *Earth-Science Reviews* **129**: 24–39.

Lomax J, Fuchs M, Antoine P et al. 2018. A luminescence-based chronology for the Harletz loess sequence, Bulgaria. *Boreas* **48**: 179–194.

Margari V, Skinner LC, Tzedakis PC *et al.* 2010. The nature of millennial-scale climate variability during the past two glacial periods. *Nature Geoscience* **3**: 127–131.

Marković SB, Oches EA, Sümegi P *et al.* 2006. An introduction to the Middle and Upper Pleistocene loess-paleosol sequence at Ruma brickyard, Vojvodina, Serbia. *Quaternary International* **149**: 80–86.

Marković SB, Oches EA, McCoy WD *et al.* 2007. Malacological and sedimentological evidence for "warm" glacial climate from the Irig loess sequence, Vojvodina, Serbia. *Geochemistry, Geophysics, Geosystems* **8**: 1–12.

Marković SB, Bokhorst MP, Vandenberghe J *et al.* 2008. Late Pleistocene loess-palaeosol sequences in the Vojvodina region, north Serbia. *Journal of Quaternary Science* **23**: 73–84.

Marković SB, Hambach U, Catto N *et al.* 2009. Middle and late pleistocene loess sequences at Batajnica, Vojvodina, Serbia. *Quaternary International* **198**: 255–266.

Marković SB, Hambach U, Stevens T *et al.* 2011. The last million years recorded at the Stari Slankamen (North Serbia) loess-paleosol sequence: Revised chronostratigraphy and long-term environmental trends. *Quaternary Science Reviews* **30**: 1142–1154.

Marković SB, Stevens T, Kukla GJ *et al.* 2015. Danube loess stratigraphy - Towards a pan-European loess stratigraphic model. *Earth-Science Reviews* **148**: 228–258.

Marković SB, Sümegi P, Stevens T *et al.* 2018. The Crvenka loess-paleosol sequence: A record of continuous grassland domination in the southern Carpathian Basin during the Late Pleistocene. *Palaeogeography, Palaeoclimatology, Palaeoecology* **509**: 33–46.

Mejdahl V. 1979. Thermoluminescence dating: Beta-dose attenuation in quartz grains. *Archaeometry* **21**: 61–72.

Moseley GE, Spötl C, Cheng H *et al.* 2015. Termination-II interstadial/stadial climate change recorded in two stalagmites from the north European Alps. *Quaternary Science Reviews* **127**: 229–239.

Murray AS, Wintle AG. 2000. Luminescence dating of quartz using an improved single-aliquot regenerative-dose protocol. *Radiation Measurements* **32**: 57–73.

Murray AS, Schmidt ED, Stevens T *et al.* 2014. Dating middle pleistocene loess from Stari Slankamen (Vojvodina, Serbia) -

limitations imposed by the saturation behaviour of an elevated temperature IRSL signal. *Catena* **117**: 34–42.
Novothny Á, Horváth E, Frechen M. 2002. The loess profile at Albertirsa, Hungary-Improvements in loess stratigraphy by luminescence dating. *Quaternary International* **95–96**: 155–163.
Novothny Á, Frechen M, Horváth E *et al.* 2009. Luminescence and amino acid racemization chronology of the loess–paleosol sequence at Süttő, Hungary. *Quaternary International* **198**: 62–76.
Novothny Á, Frechen M, Horváth E *et al.* 2010. Infrared stimulated luminescence and radiofluorescence dating of aeolian sediments from Hungary. *Quaternary Geochronology* **5**: 114–119.
Novothny Á, Frechen M, Horváth E *et al.* 2011. Investigating the penultimate and last glacial cycles of the Süttő loess section (Hungary) using luminescence dating, high-resolution grain size, and magnetic susceptibility data. *Quaternary International* **234**: 75–85.
Perić Z, Lagerbäck Adolphi E, Stevens T *et al.* 2019. Quartz OSL dating of late quaternary Chinese and Serbian loess: A cross Eurasian comparison of dust mass accumulation rates. *Quaternary International* **502**: 30–44.
Prescott JR, Hutton JT. 1994. Cosmic ray contributions to dose rates for luminescence and ESR dating: Large depths and long-term time variations. *Radiation Measurements* **23**: 497–500.
Rasmussen SO, Bigler M, Blockley SPE *et al.* 2014. A stratigraphic framework for abrupt climatic changes during the Last Glacial period based on three synchronized Greenland ice-core records: Refining and extending the INTIMATE event stratigraphy. *Quaternary Science Reviews* **106**: 14–28.
Roberts HM. 2012. Testing Post-IR IRSL protocols for minimising fading in feldspars, using Alaskan loess with independent chronological control. *Radiation Measurements* **47**: 716–724.
Roucoux KH, Tzedakis PC, Lawson IT *et al.* 2011. Vegetation history of the penultimate glacial period (Marine isotope stage 6) at Ioannina, north-west Greece. *Journal of Quaternary Science* **26**: 616–626.
Rousseau D-D, Antoine P, Hatté C *et al.* 2002. Abrupt millennial climatic changes from Nussloch (Germany) Upper Weichselian eolian records during the Last Glaciation. *Quaternary Science Reviews* **21**: 1577–1582.
Schatz A-K, Buylaert J-P, Murray AS *et al.* 2012. Establishing a luminescence chronology for a palaeosol-loess profile at Tokaj (Hungary): A comparison of quartz OSL and polymineral IRSL signals. *Quaternary Geochronology* **10**: 68–74.
Schmidt ED, Machalett B, Marković SB *et al.* 2010. Luminescence chronology of the upper part of the Stari Slankamen loess sequence (Vojvodina, Serbia). *Quaternary Geochronology* **5**: 137–142.
Stevens T, Armitage SJ, Lu H *et al.* 2006. Sedimentation and diagenesis of Chinese loess: Implications for the preservation of continuous, high-resolution climate records. *Geology* **34**: 849–852.
Stevens T, Marković SB, Zech M *et al.* 2011. Dust deposition and climate in the Carpathian Basin over an independently dated last glacial–interglacial cycle. *Quaternary Science Reviews* **30**: 662–681.
Stevens T, Buylaert J-P, Thiel C *et al.* 2018. Ice-volume-forced erosion of the Chinese Loess Plateau global Quaternary stratotype site. *Nature. Communications* **9**: 983.
Sümegi P, Gulyás S, Molnár D *et al.* 2018. New chronology of the best developed loess/paleosol sequence of Hungary capturing the past 1.1 ma: Implications for correlation and proposed pan-Eurasian stratigraphic schemes. *Quaternary Science Reviews* **191**: 144–166.
Thiel C, Buylaert J-P, Murray AS *et al.* 2011a. Luminescence dating of the Stratzing loess profile (Austria) – Testing the potential of an elevated temperature post-IR IRSL protocol. *Quaternary International* **234**: 23–31.
Thiel C, Buylaert J-P, Murray AS *et al.* 2011b. On the applicability of post-IR IRSL dating to Japanese loess. *Geochronometria* **38**: 369–378.
Thiel C, Horváth E, Frechen M. 2014. Revisiting the loess/palaeosol sequence in Paks, Hungary: A post-IR IRSL based chronology for the "Young Loess Series. *Quaternary International* **319**: 88–98.
Thomsen KJ, Murray AS, Jain M *et al.* 2008. Laboratory fading rates of various luminescence signals from feldspar-rich sediment extracts. *Radiation Measurements* **43**: 1474–1486.
Thomsen KJ, Murray AS, Jain M. 2011. Stability of IRSL signals from sedimentary K-feldspar samples. *Geochronometria* **38**: 1–13.
Tzedakis PC, Hooghiemstra H, Pälike H. 2006. The last 1.35 million years at Tenaghi Philippon: revised chronostratigraphy and long-term vegetation trends. *Quaternary Science Reviews* **25**: 3416–3430.
Újvári G, Kovács J, Varga G *et al.* 2010. Dust flux estimates for the Last Glacial Period in East Central Europe based on terrestrial records of loess deposits: A review. *Quaternary Science Reviews* **29**: 3157–3166.
Újvári G, Molnár M, Novothny Á *et al.* 2014. AMS 14C and OSL/IRSL dating of the Dunaszekcső loess sequence (Hungary): Chronology for 20 to 150ka and implications for establishing reliable age-depth models for the last 40ka. *Quaternary Science Reviews* **106**: 140–154.
Vandenberghe J, Marković SB, Jovanovič M *et al.* 2014. Site-specific variability of loess and palaeosols (Ruma, Vojvodina, northern Serbia). *Quaternary International* **334–335**: 86–93.
Vasiliniuc S, Vandenberghe DAG, Timar-Gabor A *et al.* 2012. Testing the potential of elevated temperature post-IR IRSL signals for dating Romanian loess. *Quaternary Geochronology* **10**: 75–80.
Wacha L, Frechen M. 2011. The geochronology of the "Gorjanović loess section" in Vukovar, Croatia. *Quaternary International* **240**: 87–99.
Wacha L, Mikulčić Pavlaković S, Novothny Á *et al.* 2011. Luminescence dating of Upper Pleistocene loess from the Island of Susak in Croatia. *Quaternary International* **234**: 50–61.
Wacha L, Galović L, Koloszár L *et al.* 2013. The chronology of the Šarengrad II loess-palaeosol section (Eastern Croatia). *Geologia Croatica* **66**: 191–203.
Wallinga J. 2002. Optically stimulated luminescence dating of young fluvial deposits: A review. *Boreas* **31**: 303–322.
Wintle AG. 1973. Anomalous fading of thermo-luminescence in mineral samples. *Nature* **245**: 143–144.
Wintle AG, Murray AS. 2006. A review of quartz optically stimulated luminescence characteristics and their relevance in single-aliquot regeneration dating protocols. *Radiation Measurements* **41**: 369–391.
Zeeden C, Dietze M, Kreutzer S. 2018. Discriminating luminescence age uncertainty composition for a robust Bayesian modelling. *Quaternary Geochronology* **43**: 30–39.
Zhang J, Tsukamoto S, Nottebaum V *et al.* 2015. De plateau and its implications for post-IR IRSL dating of polymineral fine grains. *Quaternary Geochronology* **30**: 147–153.